Composite Structures 331 (2024) 117888

Contents lists available at ScienceDirect

Composite Structures

journal homepage: www.elsevier.com/locate/compstruct

# Experimental and numerical investigation on bearing behavior of hybrid thin/thick-ply composite laminates

Mohamed Sahbi Loukil [a,*], Sergio Costa [b], Mats Bergwall [b], H.S. Deepthi Prasad [a], Florence Moreau [c], Mikael Segersäll [a], Zlatan Kapidzic [d], Robin Olsson [b]

[a] Division of Engineering Materials, Linköping University, SE-581 83 Linköping, Sweden
[b] RISE Research Institutes of Sweden AB, Box 857, SE-501 15 Borås, Sweden
[c] Oxeon AB, Företagsgatan 24, SE-504 64 Borås, Sweden
[d] Saab AB, SE-581 88 Linköping, Sweden

ARTICLE INFO

*Keywords:*
Thin Ply
Matrix crack
Bearing strength
Hybrid laminate
Composites

ABSTRACT

Experimental and numerical studies were carried out to characterize hybrid thin- and thick-ply composite laminates and assess modelling capabilities. Five different composite laminates were manufactured using a single material system with varying proportions of thin plies (0%, 50%, and 100% thin-ply). Bearing tests were performed and the results from the tests were investigated. The results showed that performance, in terms of bearing strength at onset of damage and ultimate bearing stress, increased proportionally with the increasing amount of thin plies within the laminate. Microscopic examination of the failure modes for all laminates was performed at the center of the hole to determine the dominant failure mode. The numerical investigation uses a highly detailed mesoscale model previously validated for crash simulations but never used successfully to bearing damage areas. The results showed a good correlation regarding both the load response and the morphology of damage.

## 1. Introduction

Composite materials have found usage in many industrial applications and more recently they are increasingly used in aerospace panels and airframes. The use of composites in the aerospace industry is justified by their excellent specific modulus and strength. When a composite laminate is loaded in tension with increasing load it will eventually fail (macroscopically). The failure is preceded by initiation and evolution of several microdamage modes and if the amount of damage increases, during for example the service life of the structure, laminate thermo-elastic properties are reduced. Several studies have been published describing the effect of damage development in composite laminates on the thermo-elastic properties [1–5]. Hence, it is desirable to suppress the damage development, especially the initiation of transverse cracks, which is typically the origin for the successive damage modes: delaminations and fiber breaks. One way to realize this effect is by reducing the thickness of the plies in the laminate which will effectively increase the transverse tensile strength of a ply. The general effect of an increased first crack formation strain in thin layers of laminates in tension is described in [6,7]. Another example of the thin-ply effect was demonstrated by Sihn et al. [8], who performed an experimental campaign comparing the mechanical properties of conventional laminates to thin-ply laminates. In this study it was observed that without special resins, the thin-ply laminate composites suppress microcracking, delamination and splitting damage for static, fatigue and impact loadings. In [9], quasi-isotropic laminates were prepared using both standard prepregs and thin-ply prepregs in order to examine the effect of ply thickness on the damage accumulation processes. Clear difference on the damage accumulation process between standard laminates and thin-ply laminates was identified; fiber fractures occurred in thin-ply laminates. The effect of ply thickness on the crack propagation mechanism was discussed by Saito et al. [10] with respect to the energy release rate of the intralaminar transverse cracks calculated using finite element analysis. They verified the crack suppression effect using thin plies and concluded that this effect is apparently caused by a decrease in the energy release rate at the crack tip in the thin layer. Numerical studies presented in [11–13] analyzing the influence of ply thickness on the in-situ strengths showed a significant improvement in transverse cracking and delamination resistance when using thin-ply based laminates.

The use of thin plies is beneficial; however, it is very costly to make a

* Corresponding author.
*E-mail address:* mohamed.loukil@liu.se (M.S. Loukil).

https://doi.org/10.1016/j.compstruct.2024.117888
Received 16 May 2023; Received in revised form 26 December 2023; Accepted 5 January 2024
Available online 6 January 2024

part with 100 % thin plies. For that reason, it is desirable to achieve a hybrid solution, where thin plies are used where they can contribute the most to the structural performance and conventional plies are used otherwise.

The work in [14,15] demonstrated that for laminates with a combination of thin and thick plies, both the amount and the distribution of thin plies influences the failure behavior and failure loads. Several experiments were performed on unnotched as well as notched and bearing loaded specimens and the effect was also found to be dependent on loading condition.

One potential application where the crack suppression characteristics of thin-ply laminates may be advantageous, is in bolted joints where composite structures are subjected to bearing loads. The effect of using thin plies to increase the bearing strength of composite laminates has been investigated in [16]. The results show that performance in terms of bearing stiffness, strength at onset of damage, and ultimate bearing stress increase proportionally to the increasing amount of thin plies within the stack. Shifting from a 100 % conventional ply laminate to a 100 % thin-ply laminate gave an increase of 47 % in the strength at onset of damage.

Due to the low tolerance to stress concentrations, notches or joints are sensitive spots of composite materials. Therefore, this area should be carefully analyzed with the support of numerical methods. Efficient models using a so-called composite colt joint element technique have proven to be efficient at capturing the load distribution [17,18]. However, the damage progression in bolted joints is less investigated due to a lack of constitutive models that can capture the physics of bearing damage and at the same time are efficient enough to obtain results in a reasonable time frame [19,20]. Recently Rouhi et al. in [21] used a 3D physically based model developed in [22] to simulate the bearing damage on hybrid metal/composite joints. Their results show that the simulations were able to capture the initial stiffness but fail to predict the strength, which is crucial for an efficient design.

In this paper, one of the layups tested experimentally, Laminate ID 5, was modelled in Abaqus Explicit. For the constitutive response of the material, we use the physically based constitutive model developed and validated for the crash of composites [23] but never applied to bearing damage. The simulation was performed in ABAQUS Explicit, and it was correlated against the experimental results. The laminate behavior is analyzed in terms of damage initiation, progression, delamination, and load response. The results show that the model can be used to help in the design since it can capture the initial stiffness, the strength, and most part of the damage progression at a reasonable accuracy.

## 2. Layups and testing

### 2.1. Material selection and layups

This study consists of 3 epoxy and carbon fiber prepreg materials provided by the Swedish SME Oxeon: TeXtreme 80 (thin-ply) weave, TeXtreme 160 (thin-ply) weave, and UD (thick-ply). For each material the theoretical fiber volume fraction is 47,3 %, 54,5 % and 56,9 % and the thickness of one layer is 40 μm, 80 μm and 128 μm respectively. TeXtreme 80 is a normal thin-ply thickness and the TeXtreme 160 is a thicker that could be used to reduce manufacturing time for layup.

With a combination of thick and thin plies, the following 5 laminates were manufactured in an autoclave.

**Laminate ID 1**: Laminate made of 50 % TeXtreme 80 (T80) and 50 % UD thick-ply.

**Laminate ID 2**: Laminate completely made of TeXtreme 80 (T80) which is 100 % T80 thin-ply.

**Laminate ID 3**: Laminate made of 50 % TeXtreme 160 (T160) and 50 % UD thick-ply.

**Laminate ID 4**: Laminate of 100 % TeXtreme 160 (T160) which is 100 % T160 thin-ply.

**Laminate ID 5**: Laminate made of 100 % UD which is 100 % thick-ply.

**Table 1**
Layups description for laminates tested.

| Laminate ID | Materials used | Lay-up Orientation Code |
|---|---|---|
| 1 | 50 % T80 | $[(0/90)_f/\mathbf{45}/(0/90)_f/\mathbf{-45}/(0/90)_f]_{3s}$ |
| 2 | 100 % T80 | $[(0/90)_f/(45/-45)_f]_{10s}$ |
| 3 | 50 % T160 | $[((0/90)_f/\mathbf{45/-45})_2/(0/90)_{f\ 2}/\mathbf{45/-45}/(0/\bar{9}0)_f]_s$ |
| 4 | 100 % T160 | $[(0/90)_f/(45/-45)_f]_{5s}$ |
| 5 | 100 % UD | $[\mathbf{0/90/45/-45}]_{3s}$ |

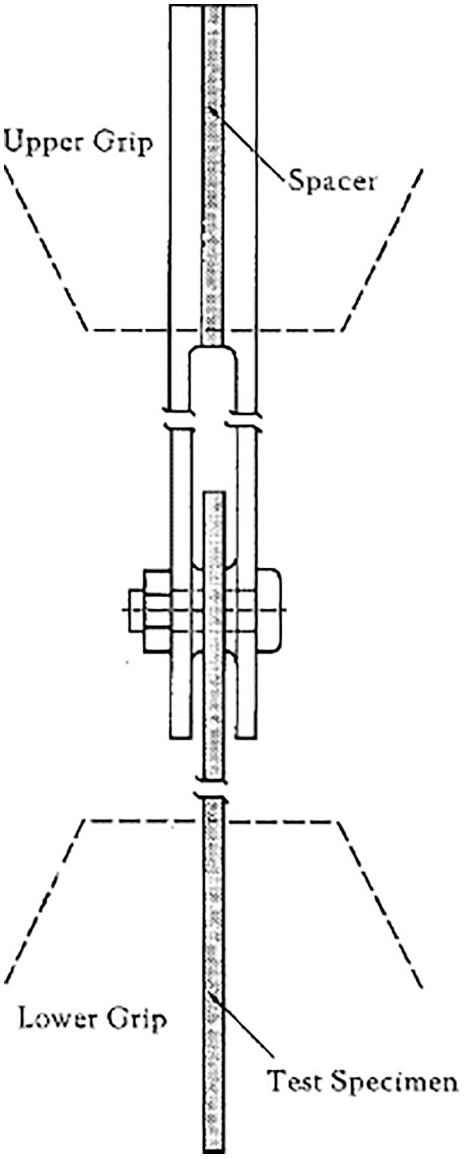


**Fig. 1.** Bearing test assembly.

Table 1 shows the layups used in testing. UD thick-ply is shown in **bold text**. Thin-plies are pre-impregnated fabrics (weave) which are marked with "$_f$". For the layup design we decided on a mixed layup where about every second layer should be a thin-ply in the hybrid layups. Also, we strived to get the same thickness for all the laminates.

### 2.2. Bearing test and standards

Bearing strength is defined as the maximum stress load that the unit can bear before the structure fails. The bearing stress of the composite laminate at each data point is calculated using equation (1) [24].

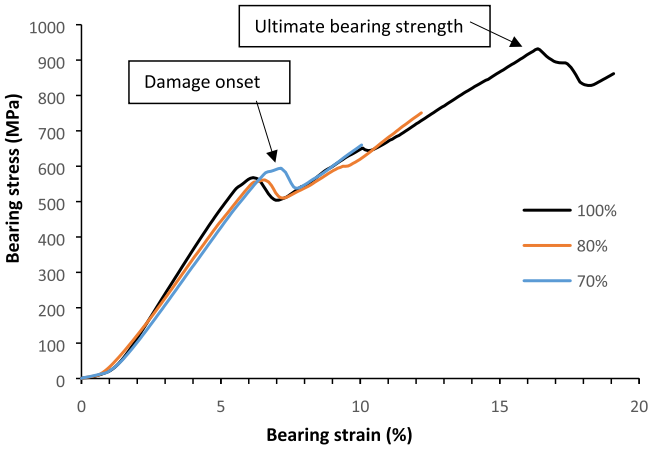


**Fig. 2.** Bearing stress/strain curve of 100% T80 loaded at 70%, 80% and 100% of its ultimate load.

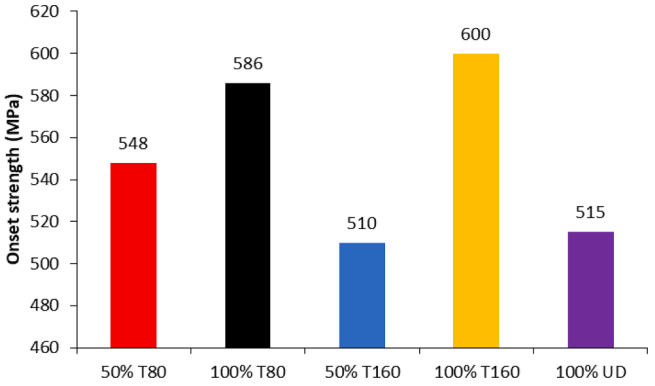


**Fig. 3.** Onset strength of all layups before compensation for fiber weight fraction.

$$\sigma = \frac{P}{k*D*h} \quad (1)$$

where $\sigma$ is the bearing stress, $P$ is the bearing force, $k$ is the force per hole factor, $D$ is the hole diameter, $h$ is the thickness of the test specimen.

Ultimate bearing strength $F$ is calculated according to equation (2) [24].

$$F = \frac{Pmax}{k*D*h} \quad (2)$$

where $Pmax$ is the maximum applied bearing force prior to bearing failure.

All mechanical testing processes follow a particular standard. Here, the bearing test is performed according to ASTM D5961. This standard consists of 4 different procedures A, B, C, D. Amongst these, procedure A, double-shear tensile loading as in Fig. 1 is used.

According to this procedure, a flat, constant rectangular cross-section specimen with the centerline hole is located near the end of the specimen and is loaded at the hole in the bearing. The bearing force is created by loading the assembly in tension in a testing machine.

## 3. Results

### 3.1. Bearing tests

The main aim of the work was to investigate the bearing strength of all the five layups mentioned above.

Fig. 2 shows an example of the bearing stress/strain curve of

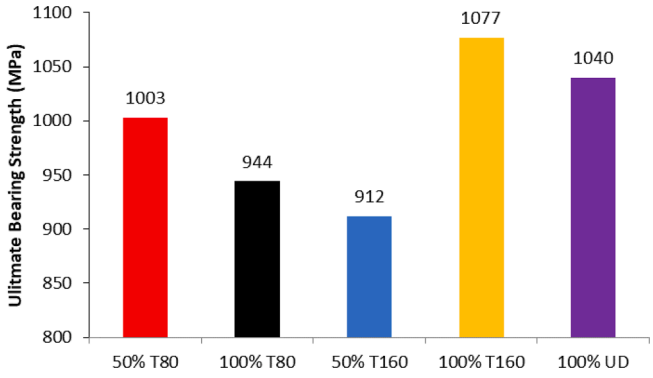


**Fig. 4.** Ultimate bearing strength of all layups before compensation for fiber weight fraction.

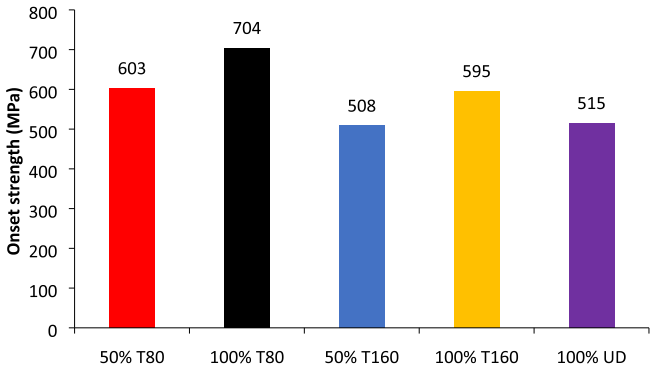


**Fig. 5.** Onset strength of all layups after compensation for fiber weight fraction.

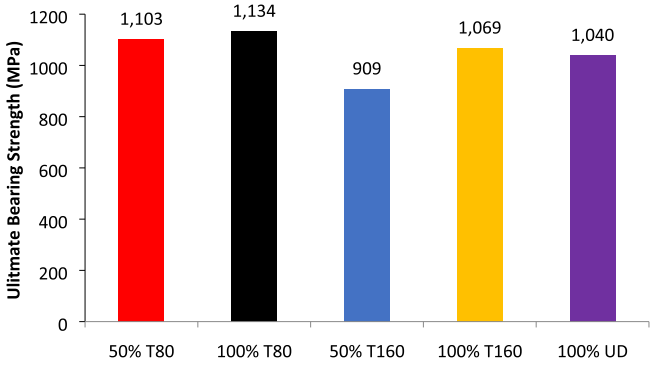


**Fig. 6.** Ultimate bearing strength of all layups after compensation for fiber.

materials which were loaded up to 70 %, 80 % and 100 % of each layup's ultimate strength. The first 8 specimens were loaded until failure, then it was decided to load one specimen to 70 % and one to 80 % of the mean ultimate strength where the test was stopped. These specimens were then examined.

Figs. 3 and 4 show the graphs of onset strength and ultimate bearing strength (UBS) respectively of all the five layups obtained from the experimental testing and without any compensation for the actual fiber weight fraction.

Figs. 5 and 6 show the graphs of onset strength and ultimate bearing strength (UBS) respectively of all the five layups obtained after the compensation made with respect to actual fiber weight fraction. This compensation was made since the different prepregs had slightly different theoretical fiber content, but also the thicknesses of the laminates after curing deviated as much as −10 % to + 25 % from expected. Therefore, the matrix burn-off method according to ASTM D2584 (Temperature 600 °C

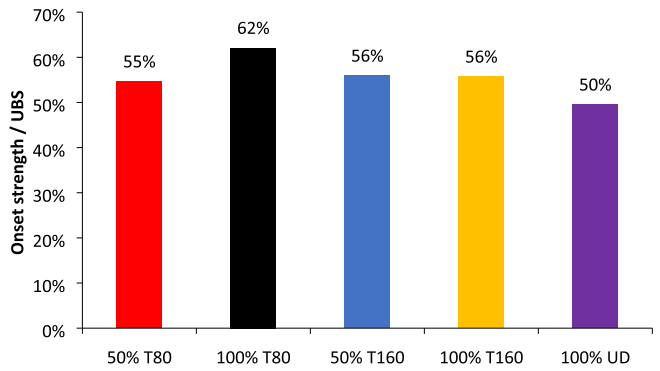


**Fig. 7.** Ratio of onset strength to ultimate bearing strength for all layups after compensation for fiber weight fraction.

and time 30 min) [25] was used to create a normalizing factor to obtain results that could be compared. For example, a laminate with excess matrix content results in a greater thickness, but the strength, when divided with thickness, suffers from the extra matrix within the sample since the fibers contribute outmost to the strength, not the matrix. Measured strengths are shown in Figs. 3 and 4 as references, where the largest compensations are for 50 % T80; +10 % and 100 % T80 about + 20 %. Compensated strengths are shown is Figs. 5 and 6.

It is clearly seen from the compiled data that the values of onset strength and the UBS of 100 % T80, with completely thin piles, is the highest.

Fig. 7 shows the ratio of the onset strength to ultimate bearing strength. It is seen that 100 % T80 has the higher ratio i.e., the onset strength to ultimate bearing strength of the layup is 62 % of the ultimate strength which is a very good value as the layup can take more load within the elastic limit when compared to the other layups and this is the greatest advantage of using the thin plies. All the other TeXtreme layups used in this work i.e., 50 % T80, 50 % 160, 100 % T160 are under the same group as they have the onset strength 55 % or more of its ultimate strength, which also are higher than UD which is 50 %. These results are independent of any fiber volume or thickness compensations.

### 3.2. Microscopic failure analysis

The major type of bearing failure mode witnessed in this work is mainly bearing and net tension failure as shown in Fig. 8.

The main objective in this section is to investigate damage at the initial point of failure and to characterize the modes of failure present in the tested specimen.

Point A in Fig. 9 shows the section where the specimens are investigated for damage under the optical microscope.

An example of microscopy image for laminate 50 % T160 is shown in Fig. 10. Fiber kinking combined with transverse cracks and delamination were observed as the main failure modes close to the hole for all samples. The interaction between these failure mechanisms forms shear cracks along the whole thickness. Similar failure modes were detected by [16,28] where damage in composite laminates was investigated as a function of applied loads in bolted joint specimens. It was shown that at very high applied bearing stress, both matrix cracking and fiber kinking were observed.

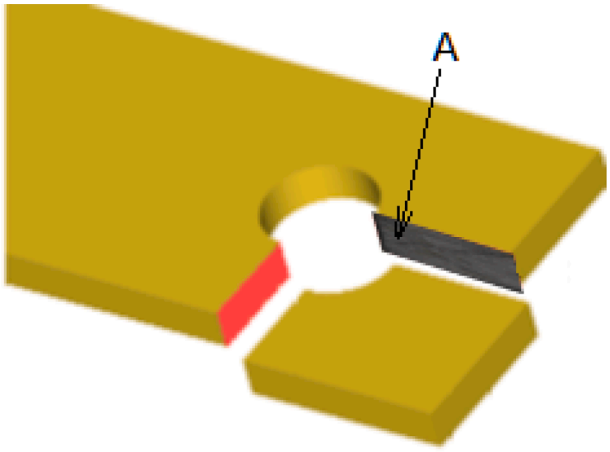


**Fig. 9.** Area investigated with the optical microscope for damage.

*a) Bearing failure (Laminate ID5)*

*b) Net tension failure (Laminate ID2)*

**Fig. 8.** Bearing failure modes in composite joints after testing (Note, tested until 1,5 mm deformation is reached).

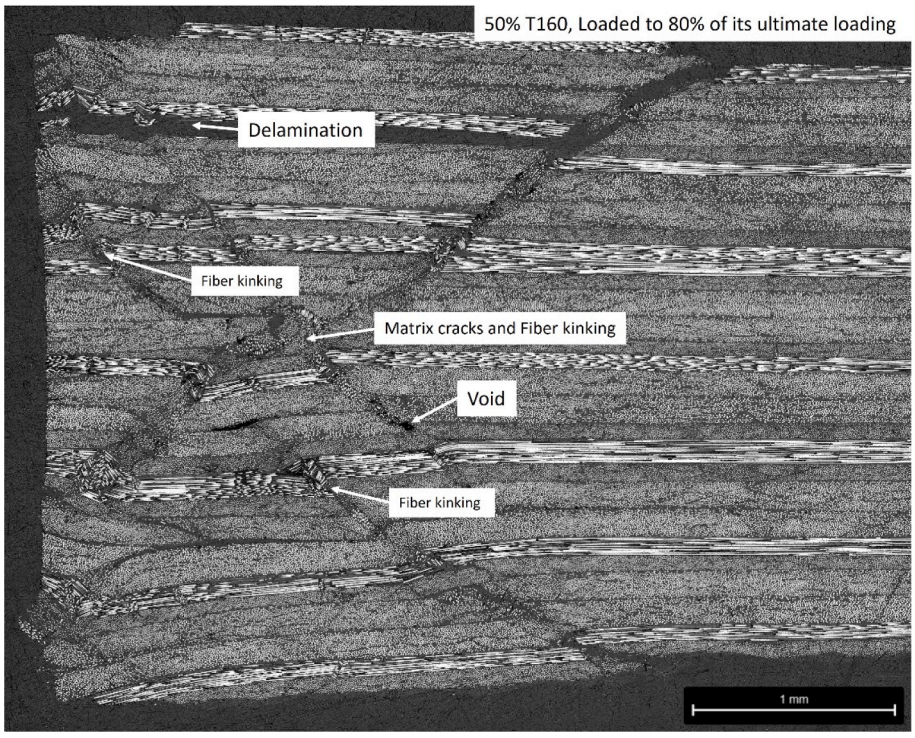


**Fig. 10.** Fractography of 50% T160 and the damage caused at 80% of its ultimate loading.

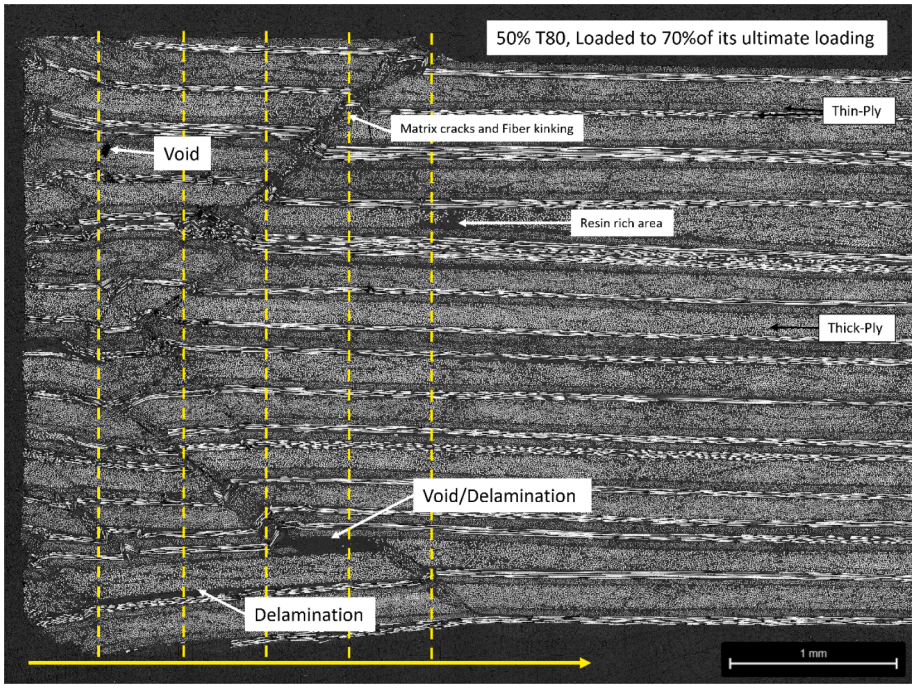


**Fig. 11.** Fractography of 50% T80 and fiber kinking caused at 70% of its ultimate loading.

All the damage mentioned above is found, but there must be a common basis to compare all the materials as they have nothing in common except for the type- and amount of fibers used and the matrix. Hence to bring this all together, the microstructure is normalized for the 2 major damage types i.e., delamination and fiber kinking. To do this, the microstructure of all the material layup is divided into 7 equal zones which are 0.5 mm apart as is shown in Fig. 11. And then, the number of fiber kinks in each zone is counted and the graph is plotted with the sum of total kinks divided by the number of 0° layers (N0°) versus the equidistant zones as it goes away from the hole edge.

A common observation of Figs. 8 and 9 is that the kink zone and resulting delaminations extend further in the plies closer to the upper and lower surfaces. This seems to be a result of the angle of the kink bands, which propagate outwards toward the unsupported free surfaces.

Fig. 12 shows the graph of normalized fiber kinking which were loaded up to 80 % of its ultimate load. It is clearly seen in the graph that

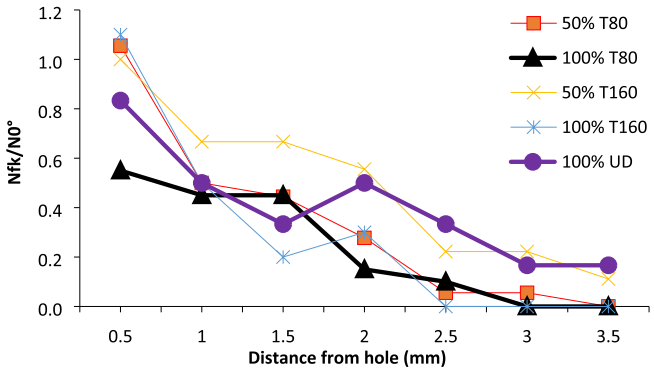


**Fig. 12.** Normalized results of fiber kinking in all the layups which were loaded up to 80% of its ultimate load.

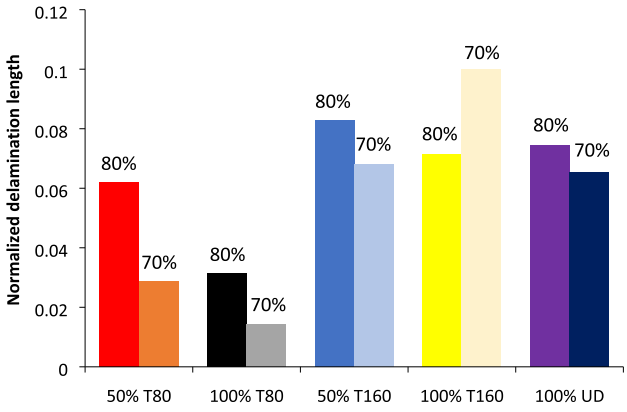


**Fig. 13.** Normalized results for delamination of all layups which were loaded up to 70% and 80%.

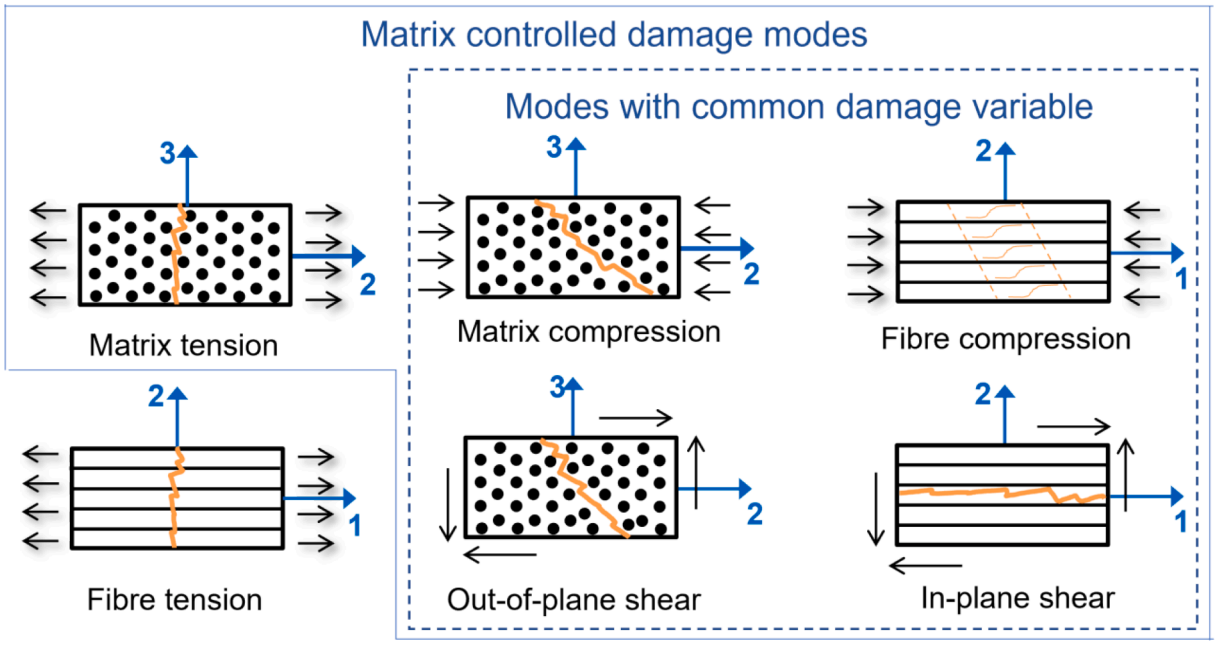


**Fig. 14.** Intralaminar damage modes accounted for in the constitutive damage model, .
adapted from [20]

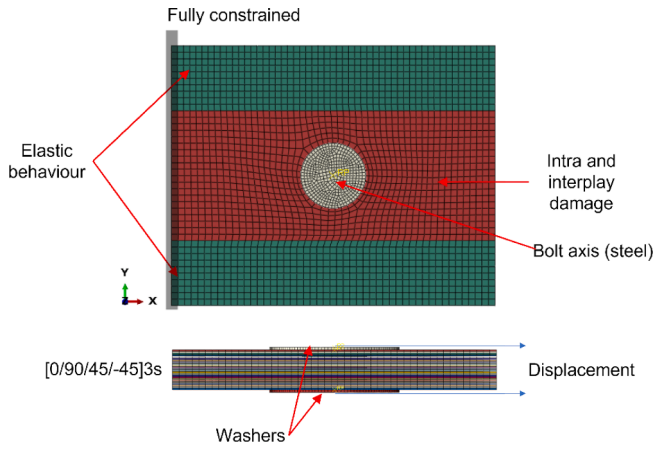


**Fig. 15.** Abaqus model with boundary conditions representative of the experiment in laminate ID5.

**Table 2**
Mechanical properties of the UD ply (laminate ID5).

| **Elastic properties** | | | | |
|---|---|---|---|---|
| Modulus (GPa) | | | Poisson's ratios | |
| $E_{11} = 137$ | $E_{22} = 10.4$ | $G_{12} = 5.2$ | $\nu_{12} = 0.3$ | $\nu_{23} = 0.5$ |
| **Strength properties** (MPa) | **Initial misalignment** | | | |
| $X_t = 2250$ | $X_c = 1400$ | $Y_t = 65$ | $\theta_i = 1^o$ | $w = 0.2$ mm |
| **Damage and friction properties** | | | | |
| Damage | Friction | | | |
| $p = -0.6$ | $\tau_o = 50$MPa | $\gamma_f = 0.6$ | $\mu = 0.4$ | $p_o = 60$Mpa |
| **Toughness properties** | | | | |
| Interlaminar toughness (kJ/m$^2$) | Interlaminar strength (MPa) | | | |
| $G_{Ic} = 1.2$ | $G_{IIc} = G_{IIIc} = 2.8$ | | $\sigma_I^o = \sigma_{II}^o = 80$ | B−K = 2.5 |
| Intralaminar toughness (kJ/m$^2$) | | Translaminar toughness (kJ/m$^2$) | | |
| $G_{Ic}^{mt} = G_{Ic}$ | | $G_c^{ft} = 85$ | $G_c^{fc} = 110$ | |

every layup follows a typical pattern where there is a downfall in the number of kinks present as it goes away from the hole. The TeXtreme material 100 % T80 has a smaller number of kinks when compared to other layups.

Fig. 13 shows the results of delamination that is normalized using Equation (3), which is obtained by counting the total length of delamination over the span from the hole edge to 3.5 mm in 0.5 mm wide zones of each specimen.

$$Normalizeddelaminationlength = \frac{\boldsymbol{Sumofdelaminationlengths}}{\boldsymbol{Totallengthofthezone}*(\boldsymbol{numberoflayers}-1)} \quad (3)$$

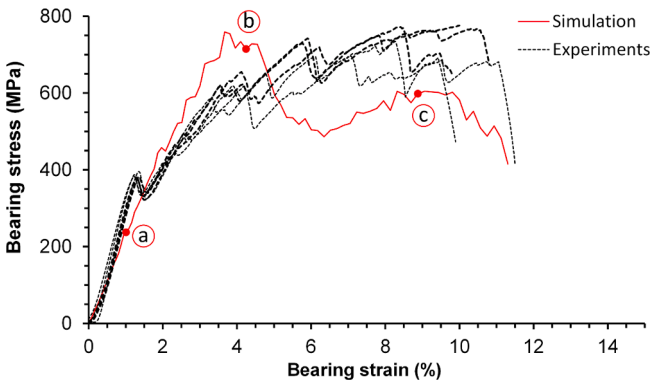


**Fig. 16.** Experiments and simulation results of the bearing stress vs. bearing strain; the 3 different markers are investigated for delaminations and bearing damage.

It is clearly visible that there is not much difference between the 70 % and 80 % of the loading and there is less delamination in 100 % T80 and has less delamination compared to other layups.

As is shown above, the use of thin plies is beneficial. The most obvious solution to increase the bearing strength is to use a laminate with 100 % thin plies. This strategy has some obvious drawbacks in terms of cost. Thin-ply materials are considered more expensive than conventional standard thickness prepreg materials. If thin-plies are used for a part, more layers are needed for the same total thickness and thus more time is required in production. For applications where performance is paramount, but costs are still required to be competitive, it would be desirable to achieve a hybrid solution, where thin plies are used where they can contribute the most performance to the structure and conventional plies are used elsewhere. One example could be edge reinforcements of panels where thin-plies are trapped-in only where the bolts are placed, as an edge reinforcement of the panel.

## 4. Numerical investigation

In this section a numerical investigation is performed to investigate whether it is possible to predict the bearing failure mechanisms visible in the experiments.

### 4.1. Overview of the constitutive model

A constitutive model previously validated for crash simulations in [23] is used here to simulate the bearing response. This model predicts the damage growth of composite materials, by considering the different interplay mechanisms occurring such as nonlinear shear, fiber kinking, matrix cracking, and fiber tensile failure. The material compressive response in the longitudinal direction is modelled with a physically based fiber kinking behavior. The formation and progression of fiber kinking is controlled by the initial fiber misalignment in interaction with matrix support. The FE-based constitutive model captures this complexity by taking advantage of the finite deformation theory to compute the nonlinear shear strain caused by the rotation of the fibers.

The matrix shear behavior is modelled by combining damage with friction as proposed by [27] with changes of damage variable, final

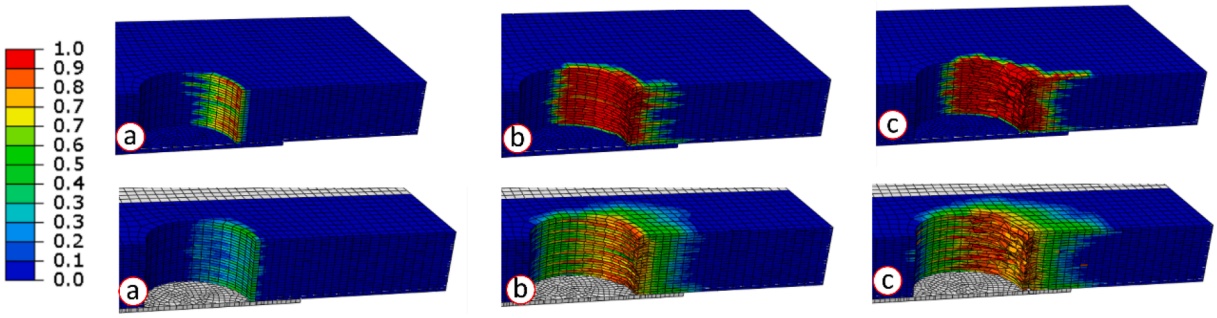


**Fig. 17.** Top row: delaminations in three stages, with 0 representing no delamination and 1 a fully delaminated interface (top ply hidden from the view); bottom row: intralaminar damage in three stages, with 0 representing no damage and 1 a fully damaged ply. Note that the top washer and half of the specimen have been removed to improve visualization.

failure criteria and interactions with matrix tension, as detailed in [23].

Furthermore, the possibility for interaction between fiber compression and matrix shear cracking is accounted for at each material point, i.e., an element undergoing fiber kinking is also experiencing matrix shear damage and vice versa. A representative interaction and competition between damage modes is fundamental to capture the mechanisms involved in damage growth and bearing failure. A schematic representation of the different damage modes and their interaction is shown in Fig. 14.

### 4.2. Bearing damage simulation

The bearing damage simulation was performed on UD laminate ID 5. A simplified model of the experimental setup (ASTM_D5961 standard) was created in Abaqus Explicit as shown in Fig. 15. Every ply was modelled with approximately 2400 3D elements with reduced integration (C3D8R) and cohesive surfaces between the plies. The elements are as regular as possible, and their length is determined by the thickness of the laminate. Note that, for a better representation of the physical test, no symmetries were applied to the model. To represent the small fiber misalignment of UD prepreg composites, an average initial fiber misalignment of 1° was used since it empirically demonstrated better results than the 3° to 4° used in previous works [23,28,29]. This difference may reflect differences in prepreg system and in the curing or layup procedure. The regions sufficiently far from the bolted joined were assigned with a linear elastic model and without cohesive surfaces to speed up the simulation, see Fig. 15. The specimen is fully constrained on one side and the load is applied on the axis of the bolt.

The material properties used in the simulation are shown were obtained from in-house measurements and are shown on Table 2. The model calibration is done by matching the in-plane shear stress of the model with the experimental in-plane shear stress as proposed in [27]. From this calibration damage and friction properties are obtained. The damage parameters are $p$, calibrated from the shear stress–strain curve; $\gamma_o$, the shear strain at onset of damage ($\gamma_o = \tau_o/G_{12}$); $\gamma_f$, the shear strain representing a fully developed shear crack. The friction parameters are the friction coefficient on the micro-crack surfaces μ, and the internal pressure $p_o$. The cohesive toughness properties used are the progressive ones instead of the initiation values. The interlaminar strength for mode II was assumed to be the same as for mode I.

### 4.3. Results - load response

The simulation takes approximately 8 h using a modern laptop with 4 CPUs. The bearing stress is plotted against the bearing strain as shown in Fig. 16. Overall, the simulation correlates well with the experiments. The initial stiffness is very well captured. The first load drop (around 400 MPa) experienced by all the experiments was not captured but instead the model predicts a gradual stiffness degradation. In fact, at point (a) the delaminations have already started accompanied by damage onset.

At point (b) the first significant drop in model has started to occur. The strength value is predicted very well but at an earlier strain than observed in the experiments. At point (c) both delaminations and damage are fully grown, and a load drop is about to occur. The experiments also start to lose load carrying capability around this level of bearing strain, although, once again, the experimental drop is more sudden while the simulation is slightly softer.

Even though the correlation is very impressive, the model predicts a stronger degradation after point (b) than the one observed in the experiments. This could be attributed to an excessive growth of delaminations and/or the interactions between cohesive modelling and ply modelling. A similar explanation has been suggested in previous work by [23] for crash simulations. It is difficult to argue that excessive delamination growth is solely responsible but with a simple examination one can see that the delaminated area is larger in the simulations than in the experiments.

The model correlation with the experiments could be further investigated by testing several coupons and stopping the tests at different loading states. The tested coupons should undergo fractography analyses to elucidate microscale damage mechanisms. Then, insights from both coupon tests and microscopy should be used to compare with the FE simulation. This would give us further insight into which mechanisms are under- or overpredicted by the model.

### 4.4. Results - morphology of damage

The aim of this section is to compare the architecture of damage in the numerical simulation and in the experiments. The different stages (a), (b) and (c) highlighted in the stress-stain plot are examined in terms of delamination and damage growth. The results are shown in Fig. 17. Note that only the upper half of the laminate is shown. Comparing stage (c) with the experimental micrograph is evident that the morphology of damage is reasonably well captured. The model predicts higher damage near the surface and shorter damage area in the middle, as observed in the micrographs.

## 5. Conclusion

Using a double lap shear loading bearing test setup, the rectangular test specimens with different lay-up sequences were loaded into the bearing through the fastener. 100 % T80 (Laminate ID2) outperformed all layups with the highest onset strength of 704 MPa and highest ultimate bearing strength of 1134 MPa when compared to all five layups. 50 % T80 (Laminate ID1) proved to be a good solution for hybrid thick/thin ply applications where production methods and cost limits the use of 100 % thin-ply layups. Fiber kinking combined with transverse cracks and delamination were observed as the main failure modes close to the

hole for all samples. Usage of thin plies improves the elastic limit of the specimen. The drop in the force/displacement graph occurring at the "damage onset" is not influenced by friction sliding in the bolt interface, bolt also prevents the laminate from expanding out-of-plane. The drop occurs due to initial fiber kinking and delaminations, which will progress with increasing load.

Due to the great complexity of bearing damage, there is a lack of predictive models in the literature. The physically based constitutive model used herein demonstrates commendable correlation with experimental data, particularly in initial stiffness and peak strength. Overall, the numerical investigation performed on laminate ID5 shows a good correlation regarding both the load response and the morphology of damage.

## CRediT authorship contribution statement

**Mohamed Sahbi Loukil:** . **Sergio Costa:** Formal analysis, Investigation, Validation, Writing – review & editing. **Mats Bergwall:** Data curation, Methodology, Writing – review & editing, Supervision. **H.S. Deepthi Prasad:** . **Florence Moreau:** Data curation, Resources. **Mikael Segersäll:** Data curation, Investigation, Supervision. **Zlatan Kapidzic:** Investigation, Writing – review & editing. **Robin Olsson:** Visualization, Writing – review & editing.

## Declaration of competing interest

The authors declare that they have no known competing financial interests or personal relationships that could have appeared to influence the work reported in this paper.

## Data availability

No data was used for the research described in the article.

## References

[1] Berthelot JM. Transverse cracking and delamination in cross-ply glass-fiber and carbon-fiber reinforced plastic laminates: static and fatigue loading. Appl Mech Rev 2003;56(1):111–47.
[2] Pakkam Gabriel VR, Loukil MS, Varna J. Analysis of intralaminar cracking in 90-plies of GF/EP laminates with distributed ply strength. J Compos Mater 2021;55 (26):3925–42.
[3] Varna J, Loukil MS, Pupurs A, Joffe R. Damage and failure analysis for composites comprehensive structural integrity V3–225 2023 - V3–246.
[4] Pupurs A, Loukil MS, Varna J. Bending stiffness of damaged cross-ply laminates. Mech Compos Mater 2021;57(1):31–46.
[5] Loukil MS, Varna J, Ayadi Z. Engineering expressions for thermo-elastic constants of laminates with high density of transverse cracks. Compos Part A: Appl Sci Manuf 2013;48(1):37–46.
[6] Parvizi A, Garrett KW, Bailey JE. Constrained cracking in glass fibre-reinforced epoxy cross-ply laminates. J Mater Sci 1978;13:195–201.
[7] Dvorak GJ. Analysis of first ply failure in composite laminates. Eng Fract Mech 1986;25:763–70.
[8] Sihn S, Kim RY, Kawabe K, Tsai SW. Experimental studies of thin-ply laminated composites. Compos Sci Technol 2007;67:996–1008.
[9] Yokozeki T, Kuoda A, Yoshimura A, Ogasawara T, Aoki T. Damage characterization in thin-ply composite laminates under out-of-plane transverse loadings. Compos Struct 2010;93:49–57.
[10] Saito H, Takeuchi H, Kimpara I. Experimental evaluation of the damage growth restraining in 90 layer of thin-ply CFRP cross-ply laminates. Adv Compos Mater 2012;21:57–66.
[11] Camanho PP, Davila CG, Pinho ST, Iannucci L, Robinson P. Prediction of in situ strengths and matrix cracking in composites under transverse tension and in-plane shear. Compos A Appl Sci Manuf 2006;37:165–76.
[12] Arteiro A, Catalanotti G, Melro A, Linde P, Camanho P. Micro-mechanical analysis of the in situ effect in polymer composite laminates. Compos Struct 2014;116: 827–40.
[13] Amacher R, Cugnoni J, Botsis J, Sorensen L, Smith W, Dransfeld C. Thin ply composites: Experimental characterization and modelling of size effects. Compos Sci Technol 2014;101:121–32.
[14] Furtado C, Arteiro A, Catalanotti G, Xavier J, Camanho pp. Selective ply-level hybridisation for improved notched response of composite laminates. Compos Struct 2016;145:1–14.
[15] Arteiro A, Catalanotti G, Xavier J, Linde P, Camanho PP. A strategy to improve the structural performance of non-crimp fabric thin-ply laminates. Compos Struct 2018;188:438–49.
[16] Cameron CJ, Larsson J, Loukil MS, Murtagh T, Wennhage P. Bearing strength performance of mixed thin/thick-ply quasi-isotropic composite laminates. Compos Struct 2021;261:113312.
[17] Belardi VG, Fanelli P, Vivio F. Theoretical definition of a new custom finite element for structural modeling of composite bolted joints. Compos Struct 2021;258: 113199.
[18] Belardi VG, Fanelli P, Vivio F. Analysis of multi-bolt composite joints with a user-defined finite element for the evaluation of load distribution and secondary bending. Compos B Eng 2021;227:109378.
[19] Qin T, Zhao L, Zhang J. Fastener effects on mechanical behaviors of double-lap composite joints. Compos Struct 2013;100:413–23.
[20] Shan M, Zhao L, Liu F, Qi D, Zhang J. Revealing the competitive fatigue failure behaviour of CFRP-aluminum two-bolt, double-lap joints 2020;244:112166.
[21] Rouhi MS, Ramantani D, Tay TE. 3D explicit simulation of bearing failure in metal–composite bolted joints. Compos Struct 2022;284:115108.
[22] Costa S, Bru T, Olsson R, Portugal A. Improvement and validation of a physically based model for the shear and transverse crushing of orthotropic composites. J Compos Mater 2018;53(12):1681–96.
[23] Costa S, Zrida H, Olsson R, Herráez M, Östlund R. A unified physically-based finite deformation model for damage growth in composites. Compos A Appl Sci Manuf 2022:161 107103.
[24] ASTM D5961/D5961M-13, Standard Test Method for Bearing Response of Polymer Matrix Composite Laminates, June 2013.
[25] ASTM D2584. Standard Test Method for Ignition Loss of Cured Reinforced Resins, September 2018.
[27] Gutkin R, Pinho ST. Combining damage and friction to model compressive damage growth in fibre-reinforced composites. J Compos Mater 2015;49(20):2483–95.
[28] Gutkin R, Costa S, Olsson R. A physically based model for kink-band growth and longitudinal crushing of composites under 3D stress states accounting for friction. Compos Sci Technol 2016:39–45.
[29] Costa S, Fagerström M, Olsson R. Development and validation of a finite deformation fibre kinking model for crushing of composites. Compos Sci Technol 2020:197–108236.